

3-2014

Improved Line Data for the Swan System $^{12}\text{C}^{13}\text{C}$ Isotopologue

Ram S. Ram

James S. A. Brooke

Peter F. Bernath

Old Dominion University, pbernath@odu.edu

Christopher Sneden

Sara Lucatello

Follow this and additional works at: https://digitalcommons.odu.edu/chemistry_fac_pubs

 Part of the [Astrophysics and Astronomy Commons](#)

Repository Citation

Ram, Ram S.; Brooke, James S. A.; Bernath, Peter F.; Sneden, Christopher; and Lucatello, Sara, "Improved Line Data for the Swan System $^{12}\text{C}^{13}\text{C}$ Isotopologue" (2014). *Chemistry & Biochemistry Faculty Publications*. 75.
https://digitalcommons.odu.edu/chemistry_fac_pubs/75

Original Publication Citation

Ram, R. S., Brooke, J. S. A., Bernath, P. F., Sneden, C., & Lucatello, S. (2014). Improved line data for the swan system $^{12}\text{C}^{13}\text{C}$ isotopologue. *Astrophysical Journal Supplement Series*, 211(1), 5. doi:10.1088/0067-0049/211/1/5

IMPROVED LINE DATA FOR THE SWAN SYSTEM $^{12}\text{C}^{13}\text{C}$ ISOTOPOLOGUE

RAM S. RAM¹, JAMES S. A. BROOKE¹, PETER F. BERNATH^{1,2}, CHRISTOPHER SNEDEN^{3,4}, AND SARA LUCATELLO⁵

¹ Department of Chemistry, University of York, Heslington, York, YO10 5DD, UK; jsabrooke@gmail.com, rr662@york.ac.uk

² Department of Chemistry & Biochemistry, Old Dominion University, 4541 Hampton Boulevard, Norfolk, VA 23529-0126, USA; pbernath@odu.edu

³ Department of Astronomy, University of Texas at Austin, Austin, TX 78712, USA; chris@verdi.as.utexas.edu

⁴ Department of Astronomy and Space Sciences, Ege University, 35100 Bornova, İzmir, Turkey

⁵ INAF, Osservatorio Astronomico di Padova, Vicolo dell'Osservatorio 5, I-35122 Padova, Italy; sara.lucatello@oapd.inaf.it

Received 2013 September 11; accepted 2013 November 19; published 2014 February 11

ABSTRACT

We present new, accurate predictions for rotational line positions, excitation energies, and transition probabilities of the $^{12}\text{C}^{13}\text{C}$ isotopologue Swan $d^3\Pi\text{-}a^3\Pi$ system 0–0, 0–1, 0–2, 1–0, 1–1, 1–2, 2–0, 2–1, and 2–2 vibrational bands. The line positions and energy levels were predicted through new analyses of published laboratory data for the $^{12}\text{C}^{13}\text{C}$ lines. Transition probabilities were derived from recent computations of transition dipole moments and related quantities. The $^{12}\text{C}^{13}\text{C}$ line data were combined with similar data for $^{12}\text{C}_2$, reported in a companion paper, and applied to produce synthetic spectra of carbon-rich metal-poor stars that have strong C_2 Swan bands. The matches between synthesized and observed spectra were used to estimate band head positions for a few of the $^{12}\text{C}^{13}\text{C}$ vibrational bands and to verify that the new computed line data match observed spectra. The much weaker C_2 lines of the bright red giant Arcturus were also synthesized in the band head regions.

Key words: line: identification – molecular data – stars: abundances – stars: carbon – stars: individual (Arcturus, HE 0212–0557)

Online-only material: color figures, machine-readable table

1. INTRODUCTION

Electronic spectra of C_2 have been studied extensively, from the near-infrared to the far-ultraviolet, and the general properties of the various band systems have been known for some time (e.g., Huber & Herzberg 1979). Of the known C_2 transitions, the Swan system ($d^3\Pi_g\text{-}a^3\Pi_u$) has been studied for more than a century. This system has been the focus of much attention mainly because of its presence in many astronomical objects including comets, interstellar clouds, late-type stars, and the Sun (Brooke et al. 2013 and references therein). The characteristic bands of the Swan system are also detected easily in hydrocarbon combustion.

In spite of much interest in the main isotopic form $^{12}\text{C}_2$, only limited laboratory data are available for the minor isotopologues, $^{12}\text{C}^{13}\text{C}$ and $^{13}\text{C}_2$. However, lines arising from $^{12}\text{C}^{13}\text{C}$ are seen in many carbon stars; therefore, accurate laboratory measurements are needed. In a previous study, Pesic et al. (1983) reported the observation of several bands of the Swan system at moderate resolution using a hollow cathode discharge of argon and ^{13}C -enriched benzene. They carried out a rotational analysis of six $^{13}\text{C}_2$ bands and the 0–1, 1–1, and 1–0 bands of $^{12}\text{C}^{13}\text{C}$. The $^{13}\text{C}_2$ bands were much stronger in their spectra, causing frequent overlapping with the rotational lines of $^{12}\text{C}^{13}\text{C}$. Recently, several $^{12}\text{C}_2$, $^{13}\text{C}_2$, and $^{12}\text{C}^{13}\text{C}$ bands of the Swan system were observed at low resolution by Dong et al. (2013) during a carbon isotope analysis experiment with laser ablation of samples containing ^{12}C and ^{13}C mixtures. In a high-resolution study, Amiot (1983) recorded spectra of the 0–0 Swan bands of $^{12}\text{C}_2$, $^{13}\text{C}_2$, and $^{12}\text{C}^{13}\text{C}$ isotopologues using a Fourier transform spectrometer (FTS). High-resolution data on bands with higher vibrational levels, ($v \geq 1$), have been lacking, and so astronomers have been forced to use approximate line positions predicted from estimated $^{12}\text{C}^{13}\text{C}$ spectroscopic constants, which are entirely based on $^{12}\text{C}_2$ spectroscopic constants and isotopic relationships.

In related work, Amiot & Verges (1982) reported an analysis of the 0–0 band of the Ballik–Ramsay system of $^{13}\text{C}_2$ and $^{12}\text{C}^{13}\text{C}$ using high-resolution spectra recorded with an FTS. This study was followed with a high-resolution analysis of 12 bands of the Ballik–Ramsay system of $^{13}\text{C}_2$ (with $v' = 0\text{--}6$, $v'' = 0\text{--}3$) and seven bands of $^{12}\text{C}^{13}\text{C}$ (with $v' = 0\text{--}3$, $v'' = 0\text{--}2$) by Islami & Amiot (1986).

Along with the major isotopologue, the minor $^{12}\text{C}^{13}\text{C}$ isotopologue has also been observed in diverse astronomical sources, and has been used to determine their $^{12}\text{C}/^{13}\text{C}$ isotopic ratios. For example, Krishna Swamy (1987) performed statistical thermodynamic calculations to compare with the moderately high-resolution observations of comet West by Lambert & Danks (1983). More recently, Rousselot et al. (2012) obtained the $^{12}\text{C}/^{13}\text{C}$ isotopic ratios of 85 ± 20 and 80 ± 20 for comet T7 (LINEAR) and comet Q4 (NEAT), respectively. Hema et al. (2012) investigated the high-resolution spectra of R Coronae Borealis stars and hydrogen-deficient carbon stars by synthesizing the 0–1, 0–0, and 1–0 bands of the Swan system for $^{12}\text{C}_2$ and $^{12}\text{C}^{13}\text{C}$.

The present work has been undertaken to predict more precise line positions of the $^{12}\text{C}^{13}\text{C}$ Swan system based on spectroscopic constants from the FTS measurements determined by Amiot and coworkers, cited above. The spectroscopic constants for $v = 1$ and 2 in the $d^3\Pi$ state were estimated using accurate $v = 0$ constants and $^{12}\text{C}^{13}\text{C}$ equilibrium constants, which were estimated from the equilibrium constants of the $^{12}\text{C}_2$ Swan system (Brooke et al. 2013) and isotopic relationships. We then applied these line data to the spectra of a carbon-rich low-metallicity star and to the well-studied K giant Arcturus.

2. METHOD OF CALCULATION

The rotational line positions of the 0–0 band of the $^{12}\text{C}^{13}\text{C}$ Swan system $d^3\Pi\text{-}a^3\Pi$ (Amiot 1983), and the 0–0, 1–0, 1–1, 2–0, 2–1, 3–1, and 3–2 bands of the Ballik–Ramsay system ($b^3\Sigma^-\text{-}a^3\Pi$) (Amiot & Verges 1982; Islami & Amiot 1986)

Table 1
Equilibrium Constants (in cm^{-1}) of the $a^3\Pi$ and $d^3\Pi$ States of $^{12}\text{C}^{13}\text{C}$

Constants	$a^3\Pi$	$d^3\Pi^a$
ω_e	1609.3651(20)	1753.6109
$\omega_e x_e$	11.21028(91)	16.2191
$\omega_e y_e$...	-0.2442
B_e	1.5692827(67)	1.687683
α_e	0.015596(11)	0.018477
$\gamma_e \times 10^5$	-0.0000271(44)	-0.000133

Note. ^a See text for details.

were fitted simultaneously using the PGOPHER program (Western 2010).⁶ In addition to new spectroscopic constants for the $b^3\Sigma^-$ state, this fit provided the constants for the $v = 0, 1,$ and 2 vibrational levels of the $a^3\Pi$ state and the $v = 0$ level of $d^3\Pi$ state. The Amiot group observed several perturbations in the two band systems. All of the lines affected by local perturbations were given lower weights in the fits and were expected to have a minimal effect on the isotopic relationships. Next, the equilibrium constants of the $a^3\Pi$ and $d^3\Pi$ states of $^{12}\text{C}^{13}\text{C}$ were calculated (Table 1) using the equilibrium constants of these states in $^{12}\text{C}_2$ (Brooke et al. 2013) and the isotopic relationships: $\omega_e^i = \rho\omega_e, \omega_e x_e^i = \rho^2\omega_e x_e, \omega_e y_e^i = \rho^3\omega_e y_e, B_e^i = \rho^2 B_e, \alpha_e^i = \rho^3\alpha_e, \gamma_e^i = \rho^4\gamma_e, D_e^i = \rho^4 D_e, \beta_e^i = \rho^5\beta_e, p_e^i = \rho^2 p_e, q_e^i = \rho^4 q_e$, where $\rho = (\mu/\mu^i)^{(1/2)}$.

The predicted $a^3\Pi$ state equilibrium constants, $\omega_e = 1609.3728 \text{ cm}^{-1}$, $\omega_e x_e = 11.2097 \text{ cm}^{-1}$, $B_e = 1.56938 \text{ cm}^{-1}$, $\alpha_e = 0.01563 \text{ cm}^{-1}$, and $\gamma_e = -2.5234 \times 10^{-5} \text{ cm}^{-1}$ agreed well with the values of $\omega_e = 1609.3651 (20) \text{ cm}^{-1}$, $\omega_e x_e = 11.21028(91) \text{ cm}^{-1}$, $B_e = 1.5692827(67) \text{ cm}^{-1}$, $\alpha_e = 0.015596(11) \text{ cm}^{-1}$, and $\gamma_e = -2.71(44) \times 10^{-5} \text{ cm}^{-1}$ obtained from the present fit. The calculated values of spectroscopic constants of the $v = 0, 1,$ and 2 levels of the $^{12}\text{C}^{13}\text{C}$ $a^3\Pi$ state, obtained using the equilibrium constants described above, also agreed well with the corresponding values obtained from our fit. Assuming that similar agreement exists for the $d^3\Pi$ state, we predicted the rotational constants for the $v = 1$ and 2 vibrational levels with respect to the $d^3\Pi$ $v = 0$ constants as determined from the least squares fit. The other constants, such as $A_v, A_{Dv}, o_v, \lambda_v,$ etc., for the $v = 1$ and 2 levels were fixed with respect to their $v = 0$ values, following the trend found in the $d^3\Pi$ state of

⁶ <http://pgopher.chm.bris.ac.uk/>

$^{12}\text{C}_2$ (Brooke et al. 2013). Tables 2 and 3 provide the observed constants for $v = 0$ and the calculated values for $v = 1$ and 2 in the $d^3\Pi$ state, along with the spectroscopic constants of the $a^3\Pi$ and $b^3\Sigma^-$ states of $^{12}\text{C}^{13}\text{C}$. The line positions in the $1-0, 1-1, 2-1,$ and $2-2$ bands of $^{12}\text{C}^{13}\text{C}$ $d^3\Pi-a^3\Pi$ transition, predicted using the constants of Tables 2 and 3, are expected to be more reliable than those calculated entirely using the isotopic relationships. The inclusion of the $0-1, 1-1,$ and $1-0$ line positions from Pesic et al. (1983) deteriorated the fit because of the large uncertainty in their measurements, which was partly due to strong overlapping from $^{13}\text{C}_2$ bands.

3. CALCULATION OF LINE STRENGTHS

The line strengths for various bands of the $d^3\Pi-a^3\Pi$ transition of $^{12}\text{C}^{13}\text{C}$ were calculated in the form of Einstein A -coefficients and oscillator strengths (f -values). Computational details for the $^{12}\text{C}_2$ Swan bands are provided by Brooke et al. (2013). The Einstein A -coefficients have been calculated using the following equation:

$$A_{J'-J''} = 3.13618932 \times 10^{-7} \tilde{\nu}_3 \frac{S_{J''}^{\Delta J}}{(2J' + 1)} |\langle \psi_{v',J'} | \mathfrak{R}_e(r) | \psi_{v'',J''} \rangle|^2 \quad (1)$$

where $S_{J''}^{\Delta J}$ is the rotational line strength factor (the Hönl-London factor), $\tilde{\nu}_3$ is the transition wavenumber (cm^{-1}), \mathfrak{R}_e is the transition dipole moment (TDM) in debye, and Einstein A values are in s^{-1} .

The potentials of the two electronic states were calculated using the *RKR* program (Le Roy 2004),⁷ with the equilibrium constants of the two electronic states of $^{12}\text{C}^{13}\text{C}$ (Table 1). The *RKR* potentials of the upper and lower states and the TDM function, $\mathfrak{R}_e(r)$ (from high-level ab initio calculations), are then employed in the *LEVEL* program (Le Roy 2007)⁸ to calculate the wave functions, $\psi_{v,J}$. We used the TDM functions provided by Schmidt & Bacskay (2007) and Kokkin et al. (2007) in our line strength calculation. The TDM matrix elements obtained from *LEVEL* for each band are then used in PGOPHER (Western 2010) for the calculation of Einstein A -values. The Einstein A -values are converted into oscillator strengths (f -values) using the

⁷ <http://scienide2.uwaterloo.ca/~rlroy/rkr/>

⁸ <http://scienide2.uwaterloo.ca/~rlroy/level/>

Table 2
The Spectroscopic Constants of the $a^3\Pi$ and $d^3\Pi$ States of $^{12}\text{C}^{13}\text{C}$

Constants ^a	$a^3\Pi$			$d^3\Pi$		
	$v = 0$	$v = 1$	$v = 2$	$v = 0$	$v = 1^b$	$v = 2^b$
T_v	0.0	1586.94453(71)	3151.4685(15)	19377.1594(22)	21097.3555	22781.8544
A_v	-15.27166(78)	-15.2584(11)	-15.2343(16)	-14.0130(43)	-13.9	-13.85
$A_{Dv} \times 10^4$	1.956(30)	1.93(30)	1.59(31)	3.93(36)	3.93	3.93
B_v	1.5614782(40)	1.5458286(43)	1.5301249(49)	1.6783998(93)	1.6594194	1.6395154
$D_v \times 10^6$	5.92776(83)	5.9380(13)	5.9479(14)	6.3418(84)	6.5235	6.7052
λ_v	-0.15368(64)	-0.15348(77)	-0.1528(14)	0.0448(21)	0.0448	0.0448
o_v	0.67076(44)	0.66805(49)	0.66352(91)	0.5907(22)	0.595	0.597
p_v	0.002226(25)	0.002273(17)	0.002461(26)	0.003542(62)	0.00354	0.00354
$q_v \times 10^4$	-4.8888(56)	-5.3670(84)	-6.003(18)	-6.634(15)	-6.65	-6.67

Notes.

^a Additional constants, $H_0 = 1.291(61) \times 10^{-12}$, $p_{D0} = -4.89(78) \times 10^{-8}$, $q_{D0} = 1.769(14) \times 10^{-8}$, $H_1 = 9.9(21) \times 10^{-13}$, $q_{D1} = 2.268(32) \times 10^{-8}$, $q_{D2} = 3.055(85) \times 10^{-8}$ for the $a^3\Pi$ state and $H_0 = 1.55(22) \times 10^{-11}$ for the $d^3\Pi$ state were also determined.

^b Fixed values; see text for details.

Table 3
The Spectroscopic Constants of the $b^3\Sigma^-$ State of $^{12}\text{C}^{13}\text{C}$

Constants	$v = 0$	$v = 1$	$v = 2$	$v = 3$
T_v	5635.15027(57)	7055.49421(47)	8454.52008(67)	9832.2947(13)
B_v	1.4331269(40)	1.4177524(40)	1.4023565(41)	1.3869552(47)
$D_v \times 10^6$	5.71904(72)	5.72882(72)	5.73592(77)	5.7448(13)
$\gamma_v \times 10^3$	-1.507(175)	-1.514(174)	-1.577(174)	-1.543(175)
λ_v	0.15067(72)	0.15294(56)	0.15341(69)	0.15715(95)

Table 4
Assignments, Wavenumbers, Excitation Energies, and Transition Probabilities of Individual $^{12}\text{C}^{13}\text{C}$ Transitions^a

Assignments								Wavenumbers					Einstein A (s^{-1})	f -value	Transition
v'	v''	J'	J''	F'	F''	p'	p''	Observed (cm^{-1})	Calculated (cm^{-1})	Residual (cm^{-1})	Lower E . (cm^{-1})				
0	0	2	3	1	1	e	e	...	19370.7339	...	-1.9280	2.617529E+06	7.470145E-03	pP1e(3)	
0	0	3	4	1	1	e	e	...	19368.3875	...	8.9471	3.359125E+06	1.044125E-02	pP1e(4)	
0	0	4	5	1	1	e	e	...	19366.1767	...	22.6651	3.647616E+06	1.192968E-02	pP1e(5)	
0	0	5	6	1	1	e	e	...	19364.1266	...	39.2790	3.777913E+06	1.278095E-02	pP1e(6)	
0	0	6	7	1	1	e	e	...	19362.2592	...	58.8343	3.841279E+06	1.331293E-02	pP1e(7)	
0	0	7	8	1	1	e	e	...	19360.5916	...	81.3680	3.872963E+06	1.366804E-02	pP1e(8)	
0	0	8	9	1	1	e	e	19359.147	19359.1360	0.0110	106.9088	3.888559E+06	1.391776E-02	pP1e(9)	
0	0	9	10	1	1	e	e	...	19357.9005	...	135.4790	3.895607E+06	1.410102E-02	pP1e(10)	
0	0	10	11	1	1	e	e	...	19356.8905	...	167.0950	3.897993E+06	1.424030E-02	pP1e(11)	
0	0	11	12	1	1	e	e	...	19356.1098	...	201.7693	3.897814E+06	1.434929E-02	pP1e(12)	

Notes.

^a v = vibrational q.n., J = rotational q.n., F = spin component, p = parity, lower E . = Lower energy level.

(This table is available in its entirety in a machine-readable form in the online journal. A portion is shown here for guidance regarding its form and content.)

following equation:

$$f_{J' \leftarrow J''} = 1.49919368 \frac{1}{\tilde{\nu}^2} \frac{(2J' + 1)}{(2J'' + 1)} A_{J' \rightarrow J''} \quad (2)$$

Complete data for the $^{12}\text{C}^{13}\text{C}$ Swan band 0-1, 0-2, 1-0, 1-1, 1-2, 2-0, 2-1, and 2-2 band transitions considered in this study are given in Table 4. The quantities include: vibrational and rotational line designations, observed and calculated wavenumbers and their differences, energy levels, Einstein A values and oscillator strengths (f -values), and summary line designations.

4. APPLICATION OF THE NEW C_2 DATA TO STELLAR SPECTRA

4.1. Generation of Line Lists

In stellar abundance analyses, one needs line lists with wavelengths, lower-state excitation energies, and transition probabilities (usually expressed as $\log gf$ values) for all relevant molecular and atomic absorbers. For C_2 , we generated a line list suitable for input to the current version of the LTE synthetic spectrum code, MOOG (Snedden 1973). The relevant quantities for each line were derived for $^{12}\text{C}_2$ from the data in the table in Appendix A of Brooke et al. (2013) and for $^{12}\text{C}^{13}\text{C}$ from the data in Table 4. The resultant line list, containing nearly 184,000 transitions, can be obtained from the authors.⁹

Wavenumbers in air were computed from the vacuum wavenumbers with the Birch & Downs (1994) corrected version of Edlén's (1966) conversion formula, and inverted to produce air wavelengths in Angstroms. For lines with laboratory detections we adopted the measured wavenumbers, and

used the predicted wavenumbers for the other transitions. We changed the lower-state energies E'' from units of cm^{-1} to eV, a common convention in astronomy. Finally, we converted the Einstein spontaneous emission coefficient A' to the commonly used gf via

$$gf = f_{J' \leftarrow J''} (2J' + 1) \quad (3)$$

The MOOG code follows the development of Schadee (1964) for diatomic molecules. His approach combined Saha and Boltzmann equations to form a transition lower-state electron number density in terms of the constituent atomic free number densities (after molecular equilibrium computations), their partition functions, and the molecular dissociation energy.

The C_2 dissociation energy is well determined (e.g., $D_0 = 6.30$ eV, Urdahl et al. 1991; 6.27 eV, Pradhan et al. 1994). We adopted $D_0 = 6.27$ eV. In the Sun, and most cool stars, the free number density of carbon depends almost entirely on the CO formation, that is

$$P(\text{C}) = p(\text{C}) + p(\text{CO}) + \text{minor species}$$

where $P(\text{C})$ is the fictitious (in the absence of any molecular or ionized species) pressure of carbon. The C_2 molecule is at most a trace constituent in typical, cool, stellar atmospheres, so its dissociation energy is unimportant for this equilibrium equation. In line-forming regions ($\tau \sim -1$) of the solar atmosphere, C_2 comprises about 0.01% of the total carbon, and in lower-pressure G-K giants the percentage of C_2 is orders of magnitude less.

Diatomic molecular partition functions mathematically cancel out in the Schadee (1964) line opacity equations. However, the partition functions for homonuclear $^{12}\text{C}_2$ and heteronuclear $^{12}\text{C}^{13}\text{C}$ differ by a factor of two because the parent molecule has half as many energy states as the isotopic form. This difference cannot be accounted for in MOOG's implementation of

⁹ <http://www.as.utexas.edu/~chris/lab.html>

the Schadee formalism (D. L. Lambert 2013, private communication; see also the discussion in Cohen et al. 2006). Since C_2 is the only homonuclear molecule of interest in stellar spectroscopic investigations, we chose to make no general alteration to the synthesis code. Rather, like Cohen et al., we simply divided the gf values computed as above by a factor of two to mimic the partition function differences. This choice is reflected in our final C_2 line list, which contains all parent and isotopic lines from this study.

4.2. C_2 Swan Bands in Carbon-enhanced Metal-poor Stars

The major absorption bands of the C_2 Swan system occur in the 4500–5700 Å spectral region. However, in stars with abundance mixes like that of the Sun, the Swan system produces relatively weak absorption features that often are significantly contaminated with or completely masked by atomic lines. The strongest Swan bands, those of the $\Delta v = 0$ sequence, occur near 5100 Å, just where the strongest MgH $A^2\Pi-X^2\Sigma^+$ bands are located (e.g., Hinkle et al. 2013 and references therein). Indeed, Swan system lines often serve as contaminants to MgH. As such, they increase the difficulty in deriving reliable Mg isotopic ratios from MgH, while not presenting enough isolated C_2 features for a reliable carbon abundance analysis. In order to make a cleaner test of our new line list, first we decided to generate synthetic spectra of the Swan bands to compare with high-resolution spectra of so-called “carbon-enhanced metal-poor” stars (CEMP; see Beers & Christlieb 2005).

Cohen et al. (2006) conducted a high-resolution spectroscopic survey of 15 CEMP stars. Their spectra, obtained with the HIRES instrument, are available in the Keck Observatory archive. The observations were made as part of the program, “The first generation of stars in the Galaxy” (PI: J. Cohen), on 2002 September 27 and 28. Five 1200 s exposures were collected, using a 0.86 slit width, which yields a spectral resolution of $R \approx 45,000$. Spectra cover the range between 3840 and 5330 Å. For more details about the observations, the interested reader is referred to Cohen et al. These archival spectra were reduced using the MAKEE¹⁰ spectrum reduction package, then continuum-normalized and shifted to rest-frame using IRAF.¹¹

All of the CEMP stars in the Cohen et al. (2006) survey are very metal-poor ($-3.30 \leq [Fe/H] \leq -1.85$), relatively warm ($4945 \text{ K} \leq T_{\text{eff}} \leq 6240 \text{ K}$) subgiants and giants ($2.0 \leq \log g \leq 3.7$). These parameters combine to yield very weak atomic absorption lines in their spectra. However, the majority of CEMP stars are also enriched in neutron-capture (n -capture) elements, most noticeably in barium ($Z = 56$), the lanthanides ($57 \leq Z \leq 71$), and lead ($Z = 82$). Transitions arising from ionized n -capture species can be seen especially in the blue-violet spectral regions. Detailed abundance studies of these kinds of CEMP stars indicate that the dominant n -capture synthesis mechanism has been the slow “ s -process” (e.g., Sneden et al. 2008 and references therein), so such stars are labeled CEMP- s .

Almost all very metal-poor halo stars have relative overabundances with respect to iron of the “ α ” elements Mg, Si, Ca, and Ti. The Cohen et al. (2006) sample is no exception, with $\langle [Mg/Fe] \rangle \sim +0.5$, but since the mean metallicity of their stars

is $\langle [Fe/H] \rangle \sim -2.1$, the total magnesium abundance is still very small, thus absorption by MgH must be very weak or completely absent. Of course, carbon is very overabundant in CEMP stars; the mean enhancement in the Cohen et al. sample is $\langle [C/Fe] \rangle \sim 1.9$ ($\langle [C/H] \rangle \sim -0.2$), making C_2 the dominant spectral feature near 5000 Å.

We inspected our set of Cohen et al. (2006) data, seeking stars with the largest C_2 absorption combined with the lowest $^{12}C/^{13}C$ ratios, in order to see the $^{12}C^{13}C$ isotopic band structures. We found clearly identifiable 1–0 and 2–1 P-branch band heads of this isotopologue in six stars, and 0–1 band heads in one star. For the 0–1 band region we added a spectrum of the CEMP subgiant, LP 625–44 (Aoki et al. 2006 and references therein), which was obtained by David Lai with Hamspec at Lick Observatory. From these spectra, we estimated the observed band head wavelength differences, $\lambda(^{12}C^{13}C) - \lambda(^{12}C_2)$. For this exercise, we defined the wavelength of deepest absorption to be the band head, which we estimated to be ~ 0.3 Å blueward of the P-branch red-edge wavelength. From the wavelength differences, we computed $^{12}C^{13}C$ band head wavelengths using the corresponding $^{12}C_2$ wavelengths derived by Brooke et al. (2013). In Table 5 we list the $^{12}C_2$ band heads from that paper, our observed stellar and predicted $^{12}C^{13}C$ band heads, our predicted isotopic shifts, and those of Petic et al. (1983). Clearly, our predicted band head positions are in good agreement with the observed ones.

We chose to concentrate on the star HE 0212–0557 to compare our predicted $^{12}C^{13}C$ line data with observations over larger wavelength ranges. For details about the model parameter and abundance determinations of this star, see Cohen et al. (2006). Briefly, they derived $T_{\text{eff}} = 5075 \text{ K}$, $\log g = 2.15$, $v_{\text{micro}} = 1.8 \text{ km s}^{-1}$, and metallicity = $[Fe/H] = -2.27$. They reported abundances for 18 other elements. Highlights for our purposes are: $[C/Fe] = 1.74$, $^{12}C/^{13}C = 3-4$, $[\alpha\text{-element}/Fe] = \{[Mg \text{ I}, Ca \text{ I}, Ti \text{ I}, Ti \text{ II}]/Fe\} = +0.2$, and $[\text{rare-earth-elements}/Fe] = \{[Ba \text{ II}, La \text{ II}, Ce \text{ II}, Pr \text{ II}, Nd \text{ II}]/Fe\} = +2.2$. The enormous overabundances of carbon and the rare-earth neutron-capture abundances definitely assign HE 0212–0557 to the CEMP- s category.

We first produced synthetic spectra with the MOOG code, generating input quantities as follows. A model atmosphere for HE 0212–0557 with the Cohen et al. (2006) parameters T_{eff} , $\log g$, $[Fe/H]$, v_{micro} was calculated by interpolating in the ATLAS model grid (Kurucz 2011 and references therein).¹² We constructed the line lists beginning with the $^{12}C_2$ and $^{12}C^{13}C$ lines described above, and added atomic lines from Kurucz’s line compendium.¹³ For most atomic lines, we adopted the transition probabilities from the Kurucz database, but for neutron-capture elements (particularly the rare-earth ions) we adopted the gf ’s determined in a series of papers by the Wisconsin atomic physics group (Sneden et al. 2009 and references therein). The computed spectra were then convolved with Gaussian functions that empirically accounted for the combined effects of the Keck spectrograph slit function and stellar macroturbulence. Finally, we compared the synthetic spectra to the observed HE 0212–0557 spectrum, which had been corrected for its apparent radial velocity and continuum-normalized.

Some illustrative spectra of $^{12}C_2$ and $^{12}C^{13}C$ bands in HE 0212–0557 are provided in Figures 1 and 2. We show spectra for small wavelength ranges that include the 0–0 and 1–1 band heads in Figure 1. Absorption by C_2 dominates the spectrum

¹⁰ Software package developed by T. A. Barlow for reduction of Keck HIRES data. Available on the Keck Observatory home page, <http://www.keckobservatory.org>.

¹¹ IRAF is distributed by the National Optical Astronomy Observatory, which is operated by the Association of Universities for Research in Astronomy, Inc., under cooperative agreement with the National Science Foundation.

¹² <http://kurucz.harvard.edu/grids.html>

¹³ <http://kurucz.harvard.edu/linelists.html>

Table 5
Calculated and Observed Band Head Positions of $^{12}\text{C}^{13}\text{C}$ and Comparison of Isotope Shifts

Band	$^{12}\text{C}_2$		$^{12}\text{C}^{13}\text{C}$				$^{12}\text{C}_2$ - $^{12}\text{C}^{13}\text{C}$ Isotope Shift			
	Brooke et al. (2013)		Observed ^a		Predicted ^a		Predicted ^a		Pesic et al. (1983)	
	(cm^{-1})	(\AA)	(cm^{-1})	(\AA)	(cm^{-1})	(\AA)	(cm^{-1})	(\AA)	(cm^{-1})	(\AA)
(0-1) ^b	17739.75	5635.492	17770.1	5625.9	17770.28	5625.810	-30.53	9.682	-30.40	9.641
(1-2)	17898.58	5585.483	17925.74	5577.020	-27.16	8.463	-27.07	8.438
(0-0)	19354.79	5165.240	19354.40	5165.344	0.39	-0.104	0.52	-0.139
(1-1)	19490.23	5129.345	19487.80	5129.985	2.43	-0.640	2.42	-0.637
(2-2)	19611.01	5097.754	19608.07	5098.519	2.94	-0.764	4.03	-1.045
(1-0) ^b	21104.15	4737.079	21071.0	4744.6	21070.54	4744.635	33.61	-7.556	34.08	-7.667
(2-1)	21201.72	4715.278	21167.2	4723.0	21167.52	4722.897	34.20	-7.619	34.14	-7.607

Notes.

^a This paper; band head positions and isotope shifts are given in wavenumbers (cm^{-1}) as well as in Angstrom units in air.

^b Isotope shifts (in \AA and cm^{-1} units) observed by Dong et al. (2013) are 9.7 \AA , -30.58 cm^{-1} for the 0-1 band and -7.5\AA , 33.35 cm^{-1} for the 1-0 bands.

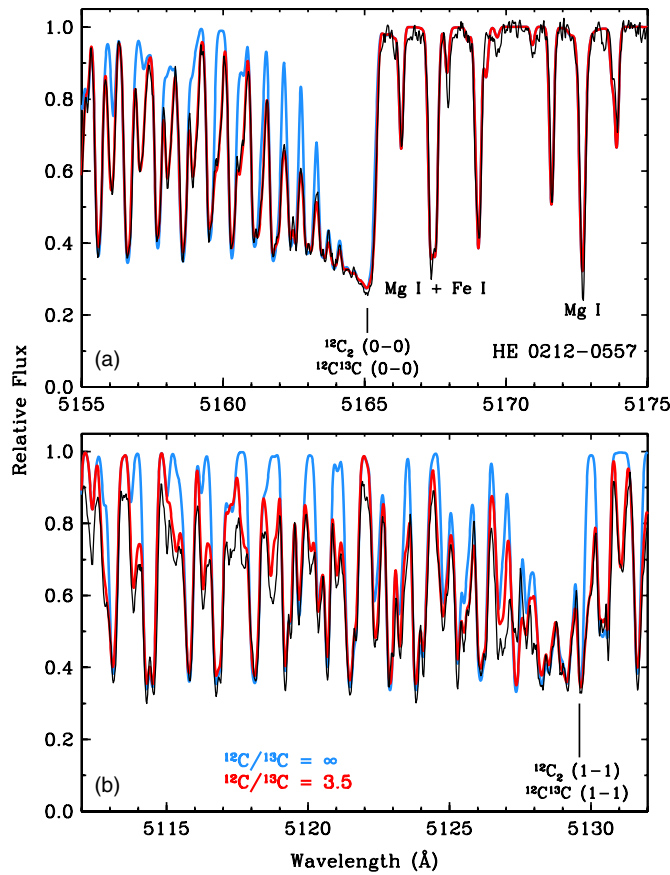


Figure 1. Observed and synthetic spectra for HE 0212-0557 around the 0-0 and 1-1 Swan system band heads. In each panel the black line is the observed spectrum. The blue line represents a synthesis with only $^{12}\text{C}_2$ lines: $^{12}\text{C}/^{13}\text{C} = \infty$. The red line represents a synthesis with substantial $^{12}\text{C}^{13}\text{C}$ contributions: $^{12}\text{C}/^{13}\text{C} = 3.5$. In panel (a) the 0-0 band head is shown, along with a small additional region to the red, without strong C_2 lines. Two Mg I b lines are labeled in the panel. In panel (b) the 1-1 band head is shown. Atomic lines are included in the syntheses, but their absorptions are overwhelmed by those of the C_2 lines. (A color version of this figure is available in the online journal.)

blueward of 5165 \AA . Isotopic wavelength shifts of the $\Delta\nu = 0$ bands are very small; the $^{12}\text{C}_2$ and $^{12}\text{C}^{13}\text{C}$ band heads are indistinguishable. Nevertheless, it is easy to see that the observed spectrum must include large contributions from $^{12}\text{C}^{13}\text{C}$ lines. We varied the carbon isotopic ratio and the total carbon abundance until the best synthetic/observed spectrum match was

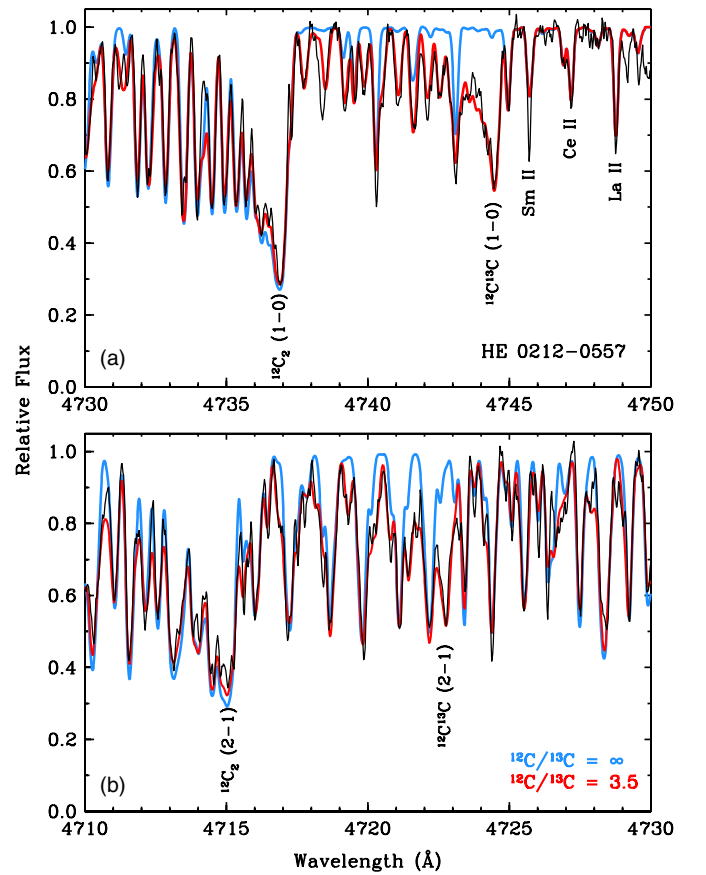


Figure 2. Observed and synthetic spectra for HE 0212-0557 around the 2-1 and 1-0 Swan system band heads. The line colors are the same as in Figure 1. Some of the atomic lines included in the syntheses have noticeable absorption. In panel (a) a few prominent rare-earth element transitions are labeled. In panel (b) note that there are many individual 1-0 transitions mixed in the 2-1 $^{12}\text{C}_2$ and $^{12}\text{C}^{13}\text{C}$ band head lines.

(A color version of this figure is available in the online journal.)

achieved, deriving $\log \varepsilon(\text{C}) = 8.12 \pm 0.05$ ($[\text{C}/\text{Fe}] = 1.8$) and $^{12}\text{C}/^{13}\text{C} \approx 4-5$. Both of these results are in excellent accord with those of Cohen et al. (2006).

Panel (a) of Figure 1 also includes a 10 \AA region redward of the 0-0 band head, which is almost devoid of C_2 absorption. Several prominent features here are due to Fe I, but there are also two of the three Mg I b lines, which are labeled in the figure. In solar

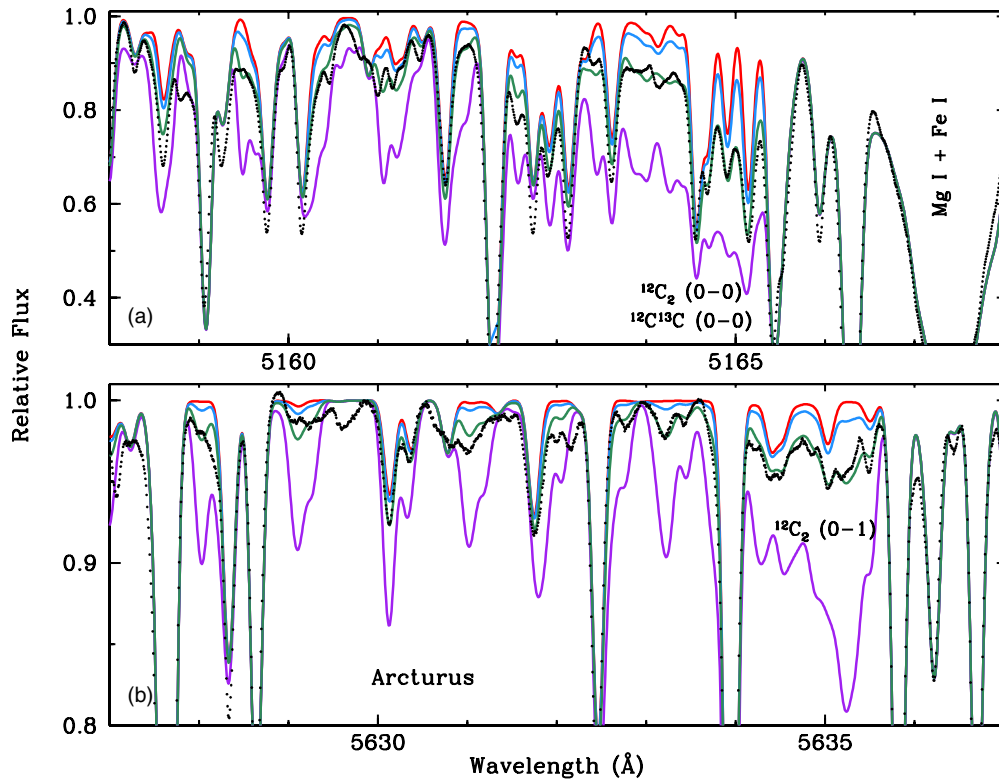


Figure 3. Observed and synthesized spectra of the 0–0 and 0–1 Swan band heads of $^{12}\text{C}_2$ and $^{12}\text{C}^{13}\text{C}$ in K-giant star Arcturus. The black dots represent the observed spectrum. The green line shows the synthesis with the best fit to the observations. The blue and purple lines represent carbon abundances reduced and increased with respect to the best fit by factors of two. The red line is a synthetic spectrum with no contribution from C_2 .

(A color version of this figure is available in the online journal.)

abundance mixtures the Mg I lines dominate the 5160–5190 Å spectral region. Their relative weakness compared to C_2 is one of the defining characteristics of an extreme CEMP star; HE 0212–0557 is a near-textbook example of such an object.

In Figure 2 we show small wavelength sections that cover the 1–0 and 2–1 band heads. Happily, the isotope shifts for the $\Delta v = +1$ sequence are large; the $^{12}\text{C}^{13}\text{C}$ band heads are about 8 Å to the red of their $^{12}\text{C}_2$ counterparts. This allows a much easier estimation of the isotopic ratio. Our derived total carbon abundance ($\log \varepsilon(\text{C}) = 8.09 \pm 0.05$) and $^{12}\text{C}/^{13}\text{C}$ ratio (4.5 ± 0.5) are indistinguishable from those obtained from the $\Delta v = 0$ bands. In panel (a) of this figure we have labeled three prominent rare-earth, ionized-species transitions. These lines would be extremely weak in metal-poor stars without the enormous overabundances of the n -capture elements of HE 0212–0557. There are other n -capture absorptions that appear among the C_2 bands; their inclusion in our syntheses improves the quality of the match to the observed spectrum. In panel (b) the $^{12}\text{C}_2$ 2–1 band head is easily identified since it dominates the absorption in the 4712–4716 Å region. One can also find the $^{12}\text{C}^{13}\text{C}$ 2–1 band head at 4722 Å, but this task is made much more difficult by the strong absorption lines in this region due to 1–0 $^{12}\text{C}_2$ and $^{12}\text{C}^{13}\text{C}$.

Our stated errors for $[\text{C}/\text{Fe}]$ and $^{12}\text{C}/^{13}\text{C}$ simply reflect uncertainties in matching the observed spectrum. Strong C_2 Swan absorption occurs throughout the 4500–5200 Å region in HE 0212–0557. This makes accurate continuum placement somewhat difficult, especially near the C_2 band heads. However, our synthetic spectra were computed over about 100 Å each in the $\Delta v = 0$ and +1 wavelength regions, and we derived consistent carbon abundances and isotopic ratios in all of the synthesized

regions. Note that our ± 0.05 error in total carbon abundance is very small because of the great sensitivity of the “double-metal” C_2 absorption to the carbon abundance. In these illustrative synthetic spectrum computations, we have not attempted to estimate the effects of model atmosphere parameters on $[\text{C}/\text{Fe}]$; see Cohen et al. (2006) for an extensive uncertainty analysis. However, we should re-emphasize statements from many past isotopic investigations: derived $^{12}\text{C}/^{13}\text{C}$ ratios are almost totally insensitive to errors in T_{eff} , $\log g$, and $[\text{M}/\text{H}]$ because the molecular parameters (dissociation and excitation energies, transition probabilities) are nearly identical for $^{12}\text{C}_2$ and $^{12}\text{C}^{13}\text{C}$.

Our HE 0212–0557 spectrum does not extend into the wavelength region of the $\Delta v = -1$ bands, which cover about 5400–5640 Å; the $^{12}\text{C}_2$ 0–1 band head lies at 5635 Å. These bands are somewhat weaker than the $\Delta v = 0$ and +1 sequences, and the isotopic shifts are to the blue. For example, the $^{12}\text{C}^{13}\text{C}$ 0–1 band head lies at 5625 Å. We synthesized this region to compare with the spectrum of another Cohen et al. (2006) star, HE 1150–0428, which has a very low $^{12}\text{C}/^{13}\text{C}$ ratio. We detected the $^{12}\text{C}^{13}\text{C}$ band head, and confirmed that our line list accurately matches the wavelengths of the observed spectrum. We concur with the Cohen et al. derived abundances ($[\text{C}/\text{Fe}] \approx +2.4$ for $[\text{Fe}/\text{H}] \approx -3.3$, and $^{12}\text{C}/^{13}\text{C} \approx 4$) in HE 0212–0557, but have no new information to add on the $\Delta v = -1$ band sequence.

4.3. C_2 in Arcturus

The very bright K-giant star Arcturus has been studied at high spectral resolution for decades. The atmospheric parameters of

this mildly metal-poor star are well known ($T_{\text{eff}} = 4300$ K, $\log g = 1.50$, $v_{\text{micro}} = 1.5$, $[\text{Fe}/\text{H}] = -0.50$; e.g., Bergemann et al. 2012). Its spectrum is used as a template for studies of other cool stars, which sometimes become differential analyses with respect to Arcturus.

The C_2 Swan bands are very weak in the Arcturus spectrum, and their lines are often completely masked by strong atomic lines. Additionally, in discussing new line data for the MgH molecule, Hinkle et al. (2013) included an estimate of the Mg isotopic fractions in Arcturus. Thus, unlike the CEMP- s star discussed in Section 4.2, the MgH lines mixed in with the C_2 $\Delta v = 0$ system in Arcturus make a carbon abundance analysis very challenging.

In Figure 3 we show synthesized and observed 0–0 and 0–1 Swan band heads in Arcturus. The observed spectrum is the very high resolution and signal-to-noise Arcturus atlas of Hinkle et al. (2000). The synthetic spectra were generated in the same manner as those of HE 0212–0557 discussed in Section 4.2. Both band heads are severely compromised with contamination by other species. In panel (a), the combined $^{12}\text{C}_2$ and $^{12}\text{C}^{13}\text{C}$ 0–0 band head near 5165.3 Å is detectable, but obviously there are cleaner C_2 features away from the band head that are better carbon abundance indicators. In panel (b), the much weaker $^{12}\text{C}_2$ 0–1 band head near 5636.5 Å is adequate for abundance studies because the atomic contamination is weak. However, we do not show the $^{12}\text{C}^{13}\text{C}$ band head near 5625.9 Å because it is completely buried underneath several strong atomic lines. Given the overall metallicity of Arcturus, ^{13}C would need to be much more abundant to be detectable with confidence in this spectral region. Even less promising are the $^{12}\text{C}_2$ and $^{12}\text{C}^{13}\text{C}$ 0–1 band heads at 4737 and 4744 Å; both are very weak and severely blended in the Arcturus spectrum. The best options for determining the carbon abundance from C_2 in this star (and others like it) appear to be individual transitions of the 0–0 band and the 0–1 band head. The $^{12}\text{C}/^{13}\text{C}$ ratios in ordinary cool giants are probably better determined from other molecular features, e.g., the CN red system.

We thank David Lambert for very helpful discussions about molecular partition functions and David Lai for sharing his spectrum of LP 625–44 with us. This work is supported in part by NSF Grant AST-1211585 to C.S. and S.L. acknowledges partial support from PRIN INAF 2011. The paper was completed while C.S. was on a University of Texas Faculty Research Assignment in residence at the Department of Astronomy and Space Sciences of Ege University. Financial support from the University of Texas and The Scientific and Technological Research Council of Turkey (TÜBİTAK, project No. 112T929) are greatly appreciated. The research at the University of York has been supported by funds from the Leverhulme Trust (UK).

Some funding was also provided by the NASA laboratory astrophysics program.

The stellar spectra data presented herein were obtained at the W. M. Keck Observatory, which is operated as a scientific partnership among the California Institute of Technology, the University of California, and the National Aeronautics and Space Administration. The Observatory was made possible by the generous financial support of the W. M. Keck Foundation.

REFERENCES

- Amiot, C. 1983, *ApJS*, **52**, 329
- Amiot, C., & Verges, J. 1982, *ApJ*, **263**, 993
- Aoki, W., Bisterzo, S., Gallino, R., et al. 2006, *ApJL*, **650**, L127
- Beers, T. C., & Christlieb, N. 2005, *ARA&A*, **43**, 531
- Bergemann, M., Hansen, C. J., Bautista, M., & Ruchti, G. 2012, *A&A*, **546**, A90
- Birch, K. P., & Downs, M. J. 1994, *Metro*, **31**, 315
- Brooke, J. S. A., Bernath, P. F., Schmidt, T. W., & Bacskay, G. B. 2013, *JQSRT*, **124**, 11
- Cohen, J. G., McWilliam, A., Shectman, S., et al. 2006, *AJ*, **132**, 137
- Dong, M., Mao, X., Gonzalez, J. J., Lu, J., & Russo, R. E. 2013, *AnaCh*, **85**, 2899
- Edlén, B. 1966, *Metro*, **2**, 71
- Hema, B. P., Pandey, D., & Lambert, D. L. 2012, *ApJ*, **747**, 102
- Hinkle, K., Wallace, L., Valenti, J., & Harmer, D. (ed.) 2000, *Visible and Near-Infrared Atlas of the Arcturus Spectrum, 3727–9300 Å* (San Francisco, CA: ASP)
- Hinkle, K. H., Wallace, L., Ram, R. S., et al. 2013, *ApJS*, **207**, 26
- Huber, K. P., & Herzberg, G. 1979, *Molecular Spectra and Molecular Structure, Volume IV: Constants of Diatomic Molecules* (New York: Van Nostrand Reinhold)
- Islami, K., & Amiot, C. 1986, *JmoSp*, **118**, 132
- Kokkin, D. L., Bacskay, G. B., & Schmidt, T. W. 2007, *JChPh*, **126**, 084302
- Krishna Swamy, K. S. 1987, *A&A*, **187**, 388
- Kurucz, R. L. 2011, *CaJPh*, **89**, 417
- Lambert, D. L., & Danks, A. C. 1983, *ApJ*, **268**, 428
- Le Roy, R. J. 2004, *RKR1 2.0: A Computer Program Implementing the First Order RKR Method for Determining Diatomic Molecule Potential Energy Functions*. University of Waterloo Chemical Physics Research Report (Waterloo, ON: Univ. Waterloo)
- Le Roy, R. J. 2007, *Level 8.0: A Computer Program for Solving the Radial Schrödinger Equation for Bound and Quasi-bound Levels*, University of Waterloo Chemical Physics Research report (Waterloo, ON: Univ. Waterloo)
- Pesic, D. S., Vujisic, B. R., Rakotoarijimy, D., & Weniger, S. 1983, *JmoSp*, **100**, 245
- Pradhan, A. D., Partridge, H., & Bauschlicher, C. W. 1994, *JCP*, **101**, 3857
- Rousselot, P., Jehin, E., Manfroid, J., & Hustemékers, D. 2012, *A&A*, **545**, A24
- Schadee, A. 1964, *BAN*, **17**, 311
- Schmidt, T. W., & Bacskay, G. B. 2007, *JChPh*, **127**, 0234310
- Snedden, C. 1973, *ApJ*, **184**, 839
- Snedden, C., Cowan, J. J., & Gallino, R. 2008, *ARA&A*, **46**, 241
- Snedden, C., Lawler, J. E., Cowan, J. J., et al. 2009, *ApJS*, **182**, 80
- Urdahl, R. S., Bao, Y., & Jackson, W. M. 1991, *CPL*, **178**, 425
- Western, C. M. 2010, *PGOPHER, A Program for Simulating Rotational Structure* (v. 7.1.108) (Bristol: Univ. Bristol)